$^{15}N(\vec{d},t)^{14}N$ at 89 MeV, j dependence and p-shell matrix elements

Swapan K. Saha, W. W. Daehnick, S. A. Dytman, P. C. Li, and J. G. Hardie
Department of Physics, University of Pittsburgh, Pittsburgh, Pennsylvania 15260

G. P. A. Berg, C. C. Foster, W. P. Jones, D. W. Miller, and E. J. Stephenson
Indiana University Cyclotron Facility, Bloomington, Indiana 47405
(Received 3 March 1989)

Differential cross sections and analyzing powers for $^{15}N(\vec{d},t)^{14}N$ were measured up to 25 MeV excitation energy with 88 and 89 MeV polarized deuteron beams and magnetic spectrographs. States of ^{14}N up to 18.53 MeV have been studied in two experiments with overall resolutions of 25–70 keV, and j transfers were determined from their characteristic analyzing powers. Mixtures of different j transfers could be determined for those 1^+ states where mixing was significant. Exact finite-range distorted-wave Born approximations calculations were used to deduce l transfers and spectroscopic strengths. The observed summed spectroscopic strength is 88% of the shell-model sum rule. Firm lower limits and tentative upper limits for six $(p_{1/2}p_{1/2})_{J,T}$ and $(p_{3/2}p_{1/2})_{J,T}$ residual two-nucleon matrix elements are deduced. Comparison with the widely used Cohen-Kurath matrix elements shows good agreement for four terms, but significant quantitative disagreement for the $(p_{1/2}p_{1/2})_{0^+,1}$ and $(p_{1/2}p_{3/2})_{1^+,1}$ terms. We also see significantly more than the predicted $p_{1/2}p_{3/2}$ mixing for the 3.948 MeV 1^+,0 state. No appreciable pickup of s-d shell admixtures was seen up to 25 MeV excitation.

I. INTRODUCTION

The p shell is a favorite "nuclear laboratory" in medium energy electron and hadron research. Approximate wave functions for these nuclei have been known for some time,[1] but it is uncertain if they are satisfactory for current demands (e.g., to deduce the contribution of meson exchange currents to form factors in electron scattering). An improved description of p-shell nuclei is highly desirable.

Large-scale shell-model calculations can treat the entire p shell quite accurately provided (a) the configuration space included is adequate and (b) the residual nucleon-nucleon interactions used are reliable. The work of Cohen and Kurath[1] deduced matrix elements and nuclear wave functions for p-shell nuclei from fits to the levels and level properties of many p-shell nuclei. The level fitting approach[1,2] is bound to suffer if levels are included in the fits which are affected by significant admixtures from configurations from higher shells. Recent shell-model calculations in an enlarged model space by Van Hees and Glaudemans,[3] who also consider 1 $\hbar\omega$ excitations, explained many observables and described most low-lying non-normal parity states in light nuclei. Their approach was later extended[4] to include 2 $\hbar\omega$ excitations, and suggested large sd configuration admixtures in the region that Cohen and Kurath had assumed to be pure p shell. Currently used p-shell matrix elements[1-3] were derived under the assumption that they are mass independent. This is contrary to the observation that matrix elements elsewhere in the Periodic Table show a very strong and smooth mass dependence, a behavior strongly suggestive of simple mass scaling.[5]

Modern experimental facilities offer fairly intense polarized beams and excellent resolution at higher energy and permit a new look at p-shell states. It has been shown that realistic diagonal matrix elements can be deduced from multiplet centroid energies computed from measured level energies and spectroscopic factors.[5] If one studies one-nucleon transfer from "one-particle" targets to two-nucleon final states, one may use the relation

$$H'_{\alpha\alpha}+E_{0\alpha}=\Sigma_\beta|\langle\phi_{0\alpha}|\Psi_\beta\rangle|^2E_\beta=\Sigma_\beta S_{\beta\alpha}E_\beta\ , \quad (1)$$

where the sum is taken over all physical nuclear states Ψ_β (with a given total angular momentum and parity J^π and with measured energies E_β) which contain some admixture of the shell-model configuration α. $E_{0\alpha}$ in Eq. (1) is the unperturbed "multiplet energy." $S_{\beta\alpha}$ are the measured and appropriately normalized spectroscopic factors, and $\{\phi_{0\alpha}\}$ is the relevant shell-model basis.

A major reason for the limited accuracy of the empirical p-shell matrix elements is our incomplete knowledge of the high-lying states. Centroids deduced for multiplets that are spread over many MeV may be skewed by missing strength at high excitation energy. Furthermore, some spectroscopic factors deduced in the past are affected by the inaccuracy of the simple separation energy method.[6]

The experiment $^{15}N(p,d)^{14}N$, was performed previously by Snelgrove and Kashy[7] with 40 MeV unpolarized protons. States of ^{14}N up to 13.74 MeV were studied with overall resolution of 90 keV. In the present $^{15}N(\vec{d},t)^{14}N$ experiment at about 90 MeV deuteron energy, our goal is to search for high-lying p strength and any

s-d strength that escaped previous observations. We also aim to use analyzing powers for the empirical unfolding of the $(p_{1/2})^2$ and $(p_{3/2},p_{1/2})$ components in 1^+ states of ^{14}N. This should provide a sensitive test of the Cohen-Kurath wave functions and matrix elements. Analyzing powers for the ^{15}N$(\vec{d},t)^{14}$N transitions have not been measured previously; however, a ^{15}N$(^3\vec{\text{He}},\alpha)^{14}$N study[8] at 33 MeV with lower resolution, but similar goals, was published in 1986.

Good discrimination between $p_{1/2}$ and $p_{3/2}$ transitions should lead to quantitative statements for well-resolved states and permit corrections for existing wave functions. Spectroscopic factors will be deduced by comparing the measured cross sections with finite-range distorted-wave Born approximations (DWBA) predictions. The experimental procedure for the present study is given in Sec. II. Section III describes results and uncertainties of this experiment. DWBA calculations, the choice of optical-model parameters, and the procedure used to deduce the contribution of different j transfers for the 1^+ states (where mixed j transfers are possible) are presented in Sec. IV. Individual levels are discussed in Sec. V. The spectroscopic factors and the deduction of p-shell matrix elements are discussed in Sec. VI.

II. EXPERIMENTAL PROCEDURE

The ^{15}N$(\vec{d},t)^{14}$N reaction was studied at the Indiana University Cyclotron Facility (IUCF) with polarized deuteron beams of 88.0 and 89.1 MeV. Beam energies are accurate to ± 0.1 MeV. The beam polarization was checked at 6 h intervals during the experiment by inserting a ^{3}He gas-cell polarimeter between the injector cyclotron and the main cyclotron and measuring the asymmetry of protons from the ^{3}He$(d,p)^4$He reaction. The polarimeter was calibrated for vector polarization using the known ratio of vector to tensor polarization from an atomic beam source and the $A_{yy}=-2$ tensor analyzing power of the ^{16}O$(d,\alpha)^{14}$N(0^+) reaction. The details are summarized in Ref. 9. The ^{15}N$(\vec{d},t)$ reaction products were studied with spectrometers; initially with the quadrupole-dipole-dipole-multipole (QDDM) magnetic spectrometer, and with the new K600 high-resolution quadrupole-dipole-dipole spectrometer after this device became available.

A. Measurements with the QDDM spectrometer

In the QDDM magnetic spectrometer, reaction particles were detected by a helical cathode position-sensitive focal plane detector. Ejectiles were identified by ΔE-ΔE measurements with two thin (1.6 and 6.4 mm) plastic scintillators located behind the helix detector. For a typical magnetic-field setting, the range of excitation energy covered by the 60 cm long helix detector was about 4.5 MeV. Hence, for each scattering angle, four magnetic-field settings were needed to cover an excitation energy range of about 17 MeV. The spectrometer entrance slits were adjusted to provide a solid angle of 1.5 msr. The angular acceptance was $\Delta\theta=1.72°$. At forward scattering angles a split Faraday cup, located inside the scattering chamber, was used. The split Faraday cup provided a way to monitor the horizontal alignment and stability of the beam. At larger scattering angles ($\theta_{\text{lab}}>20°$), an external Faraday cup located 7 m downstream from the target was used. Measurements were taken at lab angles of 10°, 15°, 20°, 23°, 27°, 30°, 35°, 40°, and 45°. The target used for the QDDM runs was a self-supporting melamine foil ($C_3H_6N_6$) of thickness 3.7 mg/cm^2. The nitrogen isotope was enriched to 99% in ^{15}N. In addition, a gas target was used for two high-excitation-energy bites. The gas cell had a diameter of 2.0 cm and was sealed by a 2.98 mg/cm^2 Havar foil. The typical gas pressure was 1.36 atm (abs).

The beam polarization fluctuated slightly ($\pm 3\%$ over several days) around the average value of $P_\uparrow=+0.553$ for "up" polarization and $P_\downarrow=-0.596$ for "down" polarization. The beam energy was measured as 87.97 MeV. Beam current was typically between 30 and 40 nA. The dead time of the data-acquisition system was measured by feeding a pulser signal, triggered by the current integrator output, through the entire electronics and computer system, and by comparing the counts in the pulser peak in the computer spectrum with the directly scaled number of pulser signals. The typical dead time encountered was about 1%. The overall resolution for the QDDM runs was 70 keV for the melamine targets, but worse for the gas target.

B. Measurements with the K600 spectrometer

The newly developed high-resolution K600 spectrometer at IUCF was used for the second phase of data taking. In the K600 spectrometer, the detector system included two vertical drift chambers (VDC) for determining the horizontal positions of the ejectiles at the focal plane, followed by two plastic scintillators (0.32 cm and 1.27 cm thick) serving as particle identifiers. As with the QDDM, for large scattering angles $\theta_{\text{lab}}>17°$, an external Faraday cup was used, whereas for forward angles an internal Faraday cup was required. The spectrograph aperture was varied depending on the scattering angle. For angles $\theta_{\text{lab}}\leq 12°$ the horizontal opening angle was $\Delta\theta=1.14°$, whereas for $\theta_{\text{lab}}>12°$ the opening angle was $\Delta\theta=3.27°$. The range of excitation energy covered at each field setting was about 14 MeV. Thus, two field settings were used to cover excitation energies of up to about 24 MeV in ^{14}N. Good energy resolution was achieved by optimizing dispersion matching with a "passive hodoscope." Procedural details are discussed in Ref. 10. The ejectile resolution ranged from 25 to 50 keV, depending on reaction angle. The data acquisition program used was "Q" (developed at Los Alamos National Laboratory, Los Alamos, New Mexico) running on a VAX 11-750 computer. This combination required limiting the counting rate to about 600 events/sec. Of the ejectiles identified as tritons, about 85% met all conditions for a "good" event. Data were taken at 6°, 9°, 12°, 15°, 17.4°, 20°, 30°, 35°, 40°, 45°, and 50°. Beam polarization remained nearly constant at $P_\uparrow=+0.522$ for "up" polarization and $P_\downarrow=-0.551$ for "down" polarization. We used two different melamine targets with nominal thicknesses 0.4 and 1.85

mg/cm^2. The 0.4 mg/cm^2 melamine target was mounted on a slotted aluminum frame with a 48 μg/cm^2 carbon backing. The 1.85 mg/cm^2 target was supported by a 45 μg/cm^2 carbon backing and had a full graphite frame. All spectra from the melamine targets contain strong ^{11}C peaks as impurity peaks. In order to identify the $^{12}C(\vec{d},t)^{11}C$ contribution from the melamine targets, data were also taken with a polystyrene target of nominal thickness 1.7 mg/cm^2. Normalized ^{11}C spectra were subtracted from the corresponding melamine spectra in the analysis. During occasional beam fluctuations the tails of the dispersed beam could strike the target holder. Such background was less disturbing for the graphite holder, although it complicated the ^{11}C normalization.

III. EXPERIMENTAL RESULTS AND ERRORS

The spin and parity of the ^{15}N ground state (g.s.) is $\frac{1}{2}^-$ and the first-order shell-model configuration for the ^{15}N g.s. is that of one $1p_{1/2}$ proton hole in a closed ^{16}O core, the neutron configuration being the same as that of ^{16}O. A pickup of a $1p_{1/2}$ neutron, therefore, populates the $J^\pi=0^+$, 1^+ states, and $1p_{3/2}$ neutron pickup populates $J^\pi=1^+$, 2^+ states of ^{14}N. Hence, we expect to see strong 0^+, 1^+, and 2^+ peaks in the ^{14}N spectra. Based upon the independent-particle shell model one expects to see six strong levels: one 0^+, $T=1$ state, two 1^+, $T=0$ states, one 1^+, $T=1$ state, one 2^+, $T=0$ state, and one 2^+, $T=1$ state.

Figure 1 shows a spectrum of $^{15}N(\vec{d},t)^{14}N$ taken at 15° with the K600 spectrometer. The $^{12}C(\vec{d},t)^{11}C$ impurity peaks from carbon in the melamine are seen and often are large. After a first-order absolute calibration, 26 peaks were identified up to 13.74 MeV excitation. More accurate excitation energies of many states were deduced by recalibrating the position spectrum with the strong, well-known levels observed.[11] The high-lying ^{14}N states are particle unstable, and at high excitations it is quite difficult to isolate the broad peaks from the continuum. The continuum "background" was determined by iterating background estimates until the total fitting error for states with known widths became comparable to the statistical fitting error. Above 13.74 MeV, eight additional peaks were identified tentatively from their known excitation energies and peak widths.[11] As expected, the strongest peaks found are those with $J^\pi=0^+$, 1^+, and 2^+.

Figure 2(a) shows a ^{11}C spectrum taken at 15° with the polystyrene target. Here we identified 11 narrow peaks with excitation energies of up to 8.655 MeV. Above this peak, we see no narrow states. The polystyrene spectra were taken in order to better evaluate the $^{15}N(\vec{d},t)^{14}N$ cross sections by subtracting these spectra from the corresponding melamine spectra. Figure 2(b) shows the subtracted spectrum obtained by subtracting the ^{11}C spectrum in Fig. 2(a) from the high-excitation-energy part of the melamine spectrum in Fig. 1.

Excitation of levels in ^{14}N by one-step pickup, other than 0^+, 1^+, or 2^+ levels, suggests s-d shell admixtures in the ground state of ^{15}N. The 2^- and 3^- peaks suggest ^{15}N ground-state admixtures of $(1d_{5/2})^2$, whereas 0^- and 1^- states indicate $(2s_{1/2})^2$ admixtures. These levels are weakly excited in ^{14}N.

The $^{15}N(\vec{d},t)^{14}N$ spectra were analyzed with the computer code AUTOFT.[12] Most peak areas were obtained by fitting the spectrum with the typical shape of strong peaks. For weakly excited levels beyond 13.74 MeV, with widths ranging from 250 to 450 keV, Gaussian peak shapes were used. Cross sections and analyzing powers were calculated from the normalized peak areas of the spin-up and spin-down spectra. The errors used were the larger of the fitting error or the statistical error. These random errors are shown in Figs. 3–10 if they exceed the

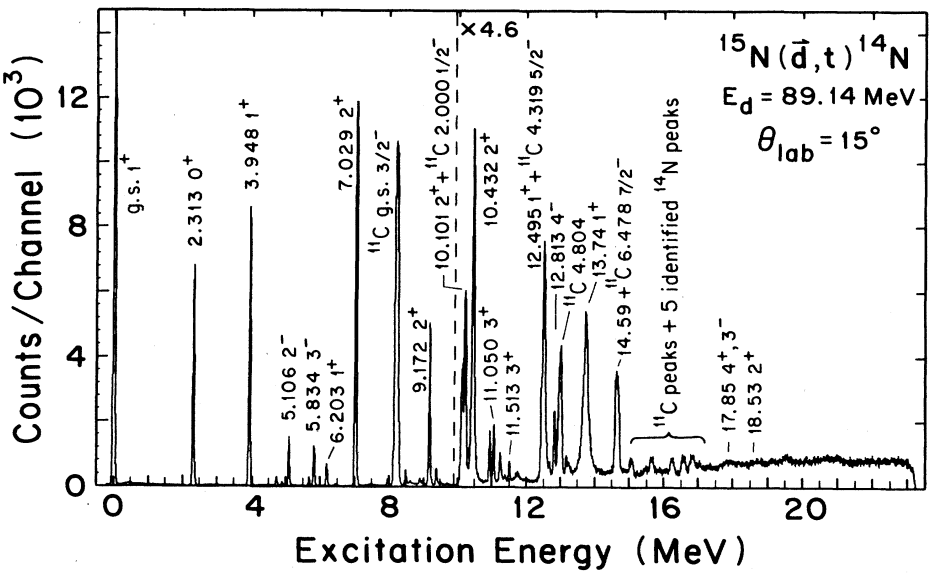

FIG. 1. Spectrum of the $^{15}N(\vec{d},t)^{14}N$ reaction at $\theta_{lab}=15°$ for $E_d=89.1$ MeV deuterons obtained with a melamine target. Impurity peaks from the $^{12}C(\vec{d},t)^{11}C$ reaction are seen at excitations above 8 MeV.

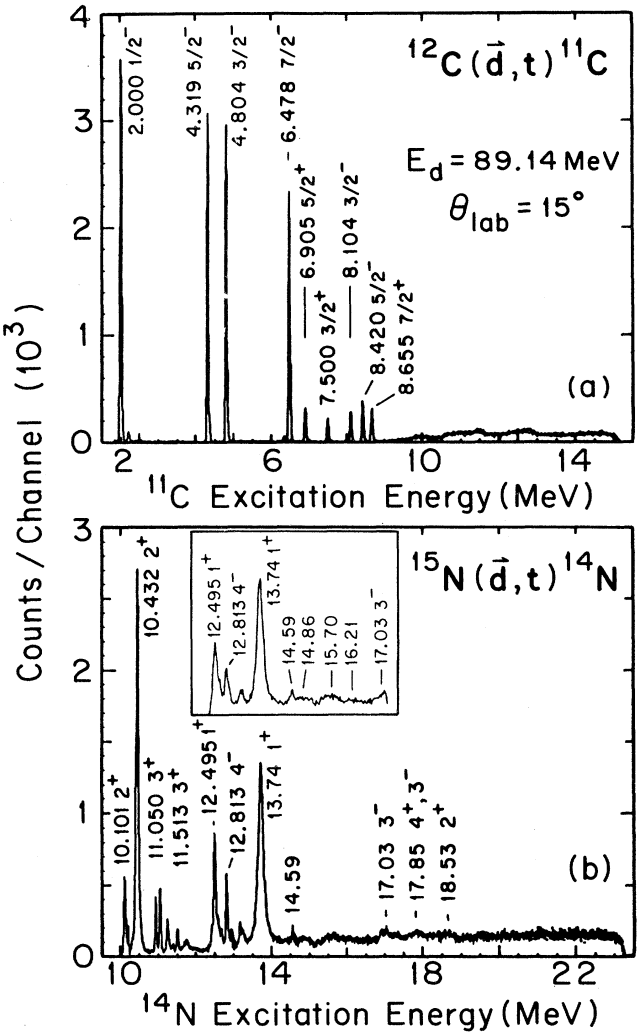

FIG. 2. (a) Spectrum of the $^{12}C(\vec{d},t)^{11}C$ reaction at $\theta_{lab}=15°$ obtained with a polystyrene target. The incident deuteron energy was $E_d=89.1$ MeV. (b) The high-excitation-energy portion of the ^{14}N aligned for ejectile energy was obtained by subtracting the ^{11}C spectrum shown in (a) from the high-excitation-energy portion of the melamine spectrum of Fig. 1. Note the absence of sharp or strong peaks from 15 to 25 MeV. The inset for (b) shows a spectrum obtained with a pure ^{15}N gas target.

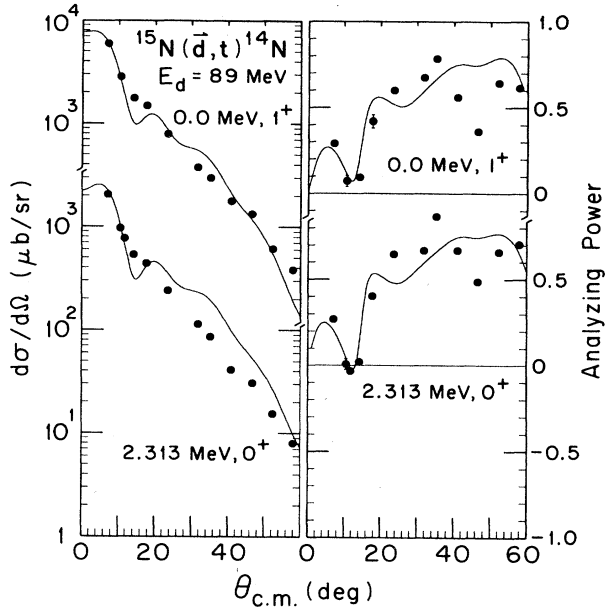

FIG. 3. Angular distributions of cross sections and analyzing powers for the ground state (1^+) and the first excited state of $^{14}N(0^+)$ at 2.313 MeV. Solid curves represent finite range DWBA calculations for $p_{1/2}$ neutron pickup.

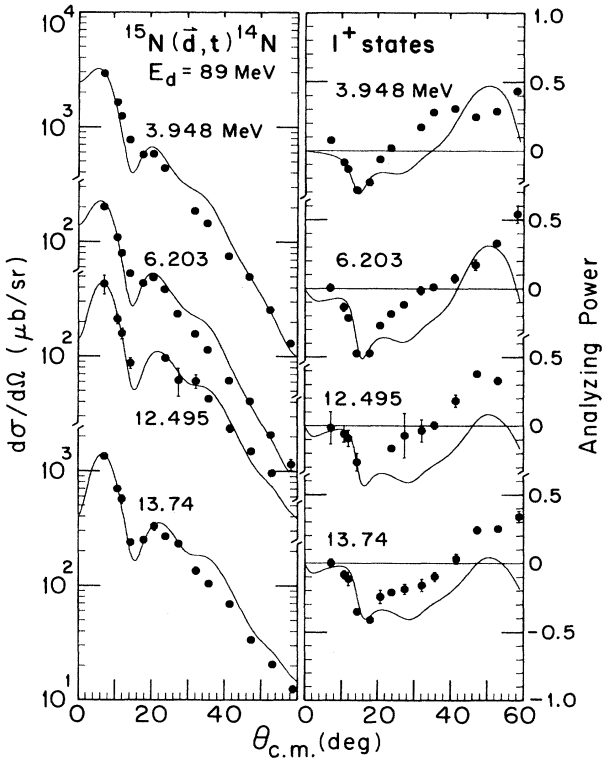

FIG. 4. Angular distributions of cross sections and analyzing powers for $J^\pi=1^+$ states of ^{14}N excited predominantly by $p_{3/2}$ neutron pickup, as indicated by the shape of the analyzing powers. Solid curves represent the calculations for $p_{3/2}$ neutron pickup, except for the 3.948 MeV state for which the DWBA curve includes a mixture of 24.3% $p_{1/2}$ pickup. All these transitions, in principle, could have $p_{1/2}$ admixtures. [See discussion in Sec. IV C.]

size of the data points.

The thicknesses of the targets were deduced by measuring the yields of elastic-scattering peaks and comparing them to previous data and optical-model predictions.[13] Statistical errors for the elastic-scattering yield were made small by acquiring good statistics. The absolute normalization error comes mainly from the uncertainties of the optical-model predictions. We estimate this error as ±15%. Table I shows a list of all states that were identified in the present experiment. The known excitation energies (column 1) and spins and parities for these states are taken from Ref. 11. The excitation ener-

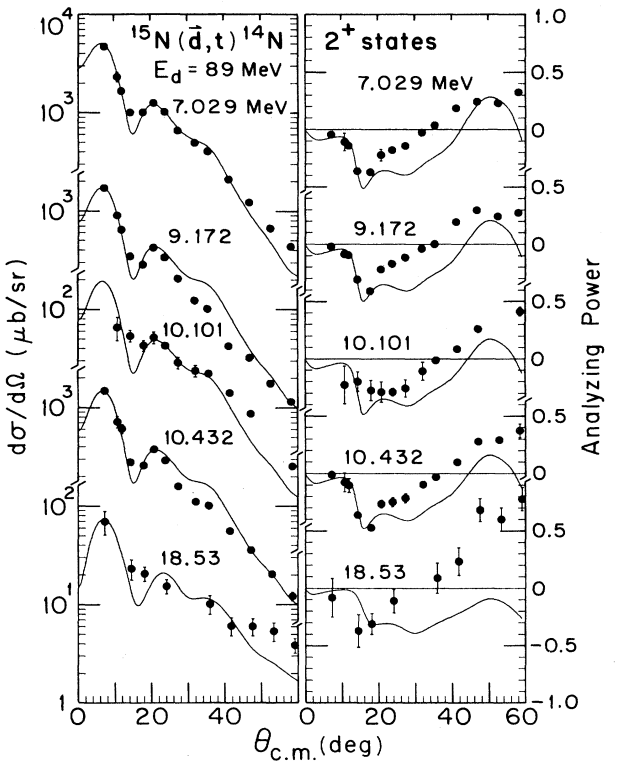

FIG. 5. Angular distributions of cross sections and analyzing powers for transitions to $J^\pi=2^+$ states of ^{14}N observed in the present experiment, which should be excited by pure $p_{3/2}$ transfer. Solid curves represent DWBA calculations for $p_{3/2}$ neutron pickup.

gies for ^{14}N states obtained in this experiment are also listed. The smaller uncertainties in excitation energies of most of the high-lying states were obtained by calibrating the spectra using sharp ^{11}C peaks near that region. Out of a total of 34 states, 11 have been identified as 0^+, 1^+, or 2^+ states, consistent with previous observations.[1,7] For the 12.495 MeV state no previous J^π value was assigned. The state at 11.513 MeV was previously assigned as either 2^+ or 3^+, the 18.53 MeV state as either 2^+ or 3^- and the 10.101 MeV state as 1^+ or 2^+. Angular distributions of cross sections (σ) and vector analyzing powers (A_y) for the 0^+, 1^+, or 2^+ states are shown in Figs. 3–5, along with DWBA calculations. Angular distributions of $\sigma(\theta)$ and A_y for weakly excited levels are shown in Figs. 6–10.

IV. DWBA ANALYSIS AND EMPIRICAL UNFOLDING OF j TRANSFERS

A. Optical-model parameters

Distorted-Wave Born approximation calculations have been carried out with the zero-range code DWUCK4 and the finite-range code FRUCK2.[14] We get reasonably good agreement for the differential cross sections, but the DWBA predictions for the analyzing powers show only qualitative agreement with the data for $\theta_{c.m.} > 20°$. This is true for both zero-range and finite-range calculations.

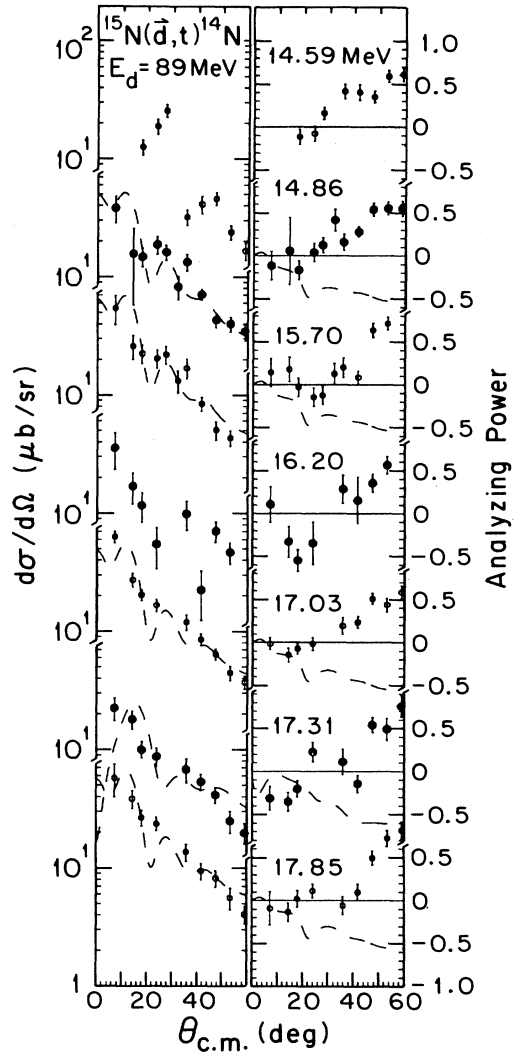

FIG. 6. Angular distributions of cross sections and analyzing powers for ^{14}N levels observed above the broad 13.74 MeV peak. None of them agree with characteristic $l=1$ shapes. The dotted curves are $l=2$ calculations, except for the $l=3$ curves at 17.31 MeV.

The D-state part of the finite-range (d,t) form factor,[14] when added to the dominant S state part, produced only a slight modification. Figure 11 shows a comparison of the zero-range and finite-range predictions for the strong 2.313 MeV 0^+ and 7.029 MeV 2^+ states.

In order to test for parameter sensitivities, different sets of optical-model potentials were tried. The form of the potential used here is as given in Ref. 13. The entrance channel optical parameters used were taken from the global parameters of Daehnick, Childs, and Vrcelj.[13] As no triton elastic-scattering data exist for lighter nuclei in the energy region of interest, we used the 79 MeV optical-model potentials for $^{16}O(^3He,^3He)$ from Ref. 15. Two different sets of parameters fit the ^3He elastic-scattering data. They differed in well depth, and were identified as the shallow (S), and the deep (D) potential.[15] We also tried an extrapolation of the (low energy)

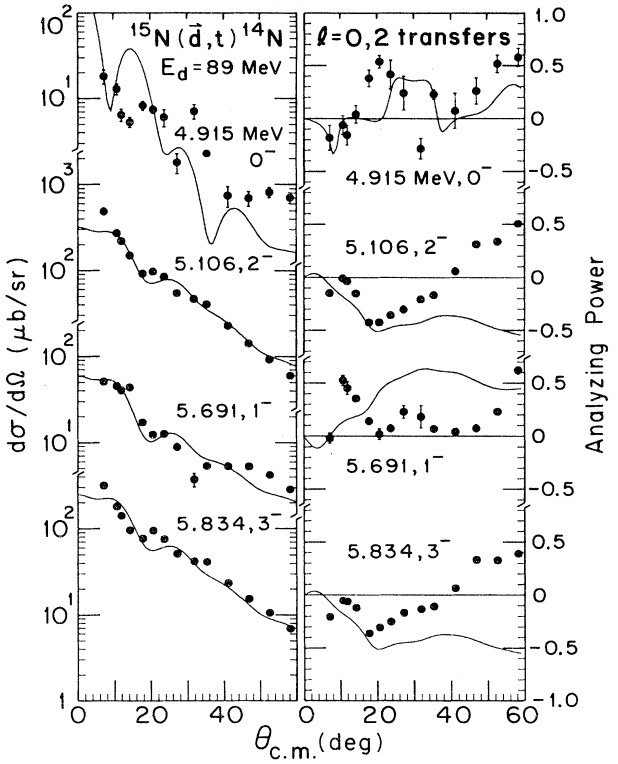

FIG. 7. Angular distributions of cross sections and analyzing powers of the lowest-lying negative-parity states excited in this reaction. The solid curves represent DWBA calculations for $2s_{1/2}$ pickup for the 4.915 MeV state, $1d_{3/2}$ pickup for the 5.691 MeV state and $1d_{5/2}$ pickup for the 5.106 and 5.834 MeV states, as suggested by selection rules. Analyzing powers show poor agreement.

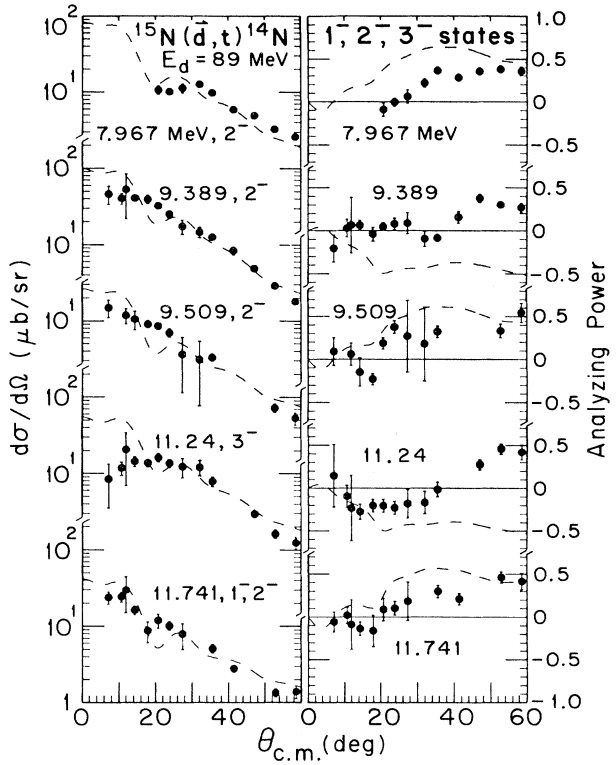

FIG. 8. Angular distributions of cross sections and analyzing powers for higher-lying, weakly excited negative-parity states of ^{14}N.

Becchetti-Greenlees global parameters[16] for tritons. The DWBA results for these three sets of parameters are shown for the 2.313 and 7.029 MeV states in Fig. 12. Consistent with earlier experience,[15–19] the deep potential gives the best fit.

We have tried other sets of best-fit optical-model (OM) parameters for both deuterons and tritons, with no significant improvement. Elastic-scattering data of ^{3}He exist[19–22] for ^{12}C at 82.1 and 70 MeV, and for ^{40}Ca at 83.5 and also at 109 MeV. For deuterons, elastic-scattering data exist[18,19,23] for ^{40}Ca at 80 MeV, for ^{12}C at 82 MeV, and for ^{16}O at 82 MeV. None of these best-fit OM parameters improved the fits to the analyzing powers. In the process we found that the shape of the analyzing power depends more strongly on the choice of triton parameters than on the choice of deuteron parameters.

B. Reaction calculations

Exact finite-range DWBA calculations were made for each observed level with the optical-model parameter sets 1 and 5 in Table II for deuterons and tritons, respectively. Spectroscopic strengths G were extracted by comparing the experimental cross section and the predicted cross section of the finite-range code FRUCK2, using the relation

$$(d\sigma/d\Omega)_{\text{pickup}} = gG(d\sigma/d\Omega)_{\text{FRUCK2}} ,$$

where $(d\sigma/d\Omega)_{\text{pickup}}$ is the experimental pickup cross section, $(d\sigma/d\Omega)_{\text{FRUCK2}}$ is the predicted cross section of the code FRUCK2 and g is the light-particle spectroscopic strength,[24] which for this reaction is $\frac{3}{2}$. For pickup the nuclear spectroscopic strength G is equal to C^2S, where C is an isospin Clebsch-Gordan coefficient and S is the spectroscopic factor.

In FRUCK2 the bound-state wave function of the transferred neutron is generated with a Woods-Saxon potential well, the depth of which is adjusted to match the separation energy of the neutron. The bound-state potential-well radius (r_0) and diffuseness (a_0) parameters were fixed at 1.28 and 0.85 fm, respectively, the smallest geometry to yield spectroscopic factors for the $p_{1/2}$ orbit which stayed within the shell-model sum rules. Spectroscopic strengths computed with the more typical well parameters of $r_0=1.20$ fm and $a_0=0.75$ fm *exceeded* the shell-model limit by 17%. [For nucleon scattering above 20 MeV, this (1.20, 0.75) well geometry was preferred[25] over two other widely used sets of well parameters, $r_0=1.25$, $a_0=0.65$, and $r_0=1.20$, $a_0=0.65$. For the latter, computed spectroscopic strengths here exceeded the sum rule by 23 and 37%, respectively.] In all DWBA calculations we computed the neutron form factor by the surface-peak method, i.e., the refined approach

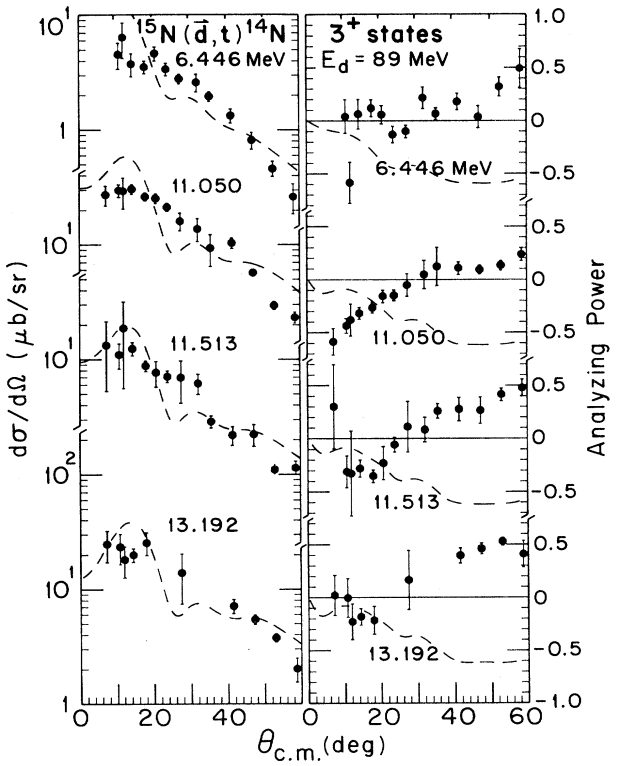

FIG. 9. Angular distributions of cross sections and analyzing powers for the 3^+ states of ^{14}N excited in the present experiment. In one-step transfers these levels can only be excited by $f_{7/2}$ pickup. The $l=3$ calculations (shown) gave poor fits.

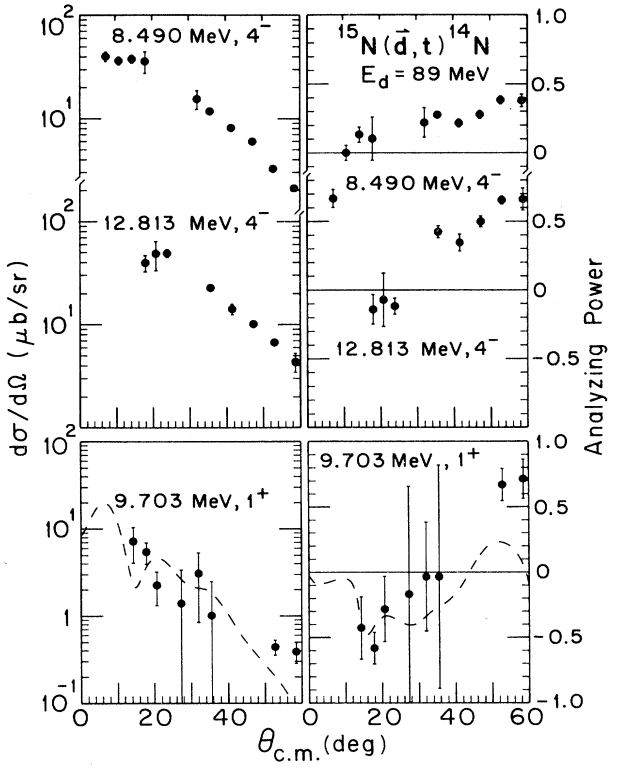

FIG. 10. Angular distributions of cross sections and analyzing powers for very weak 4^- and 1^+ state of ^{14}N, which are probably excited by multistep transfer.

suggested by Austern and Rae.[6,26] We note that differences from the separation energy method in this case were $\leq 1\%$. The spin-orbit parameter λ was kept fixed at 20.

[The rms charge radius of ^{14}N calculated from the adopted well geometry (1.28, 0.85) and independent particle model (IPM) wave functions was somewhat larger than the value of 2.54 ± 0.02 fm obtained from electron scattering.[27] This means the electron data favor a smaller well geometry (and hence *larger* spectroscopic factors), whereas the spectroscopic sum rules demand a well at least as large as the one used.]

It is widely recognized that the conventional well-parameter values, although used extensively at lower bombarding energies, are somewhat arbitrary. Different "reasonable" choices may result in spectroscopic strengths differing by 25%.[28] We also tried the extrapolated geometrical parameters of Streets, Brown, and Hodgson,[29] $r_0=1.285$ fm and $a_0=0.659$ fm, with $V_{LS}=12$ MeV, $r_{LS}=1.1$ fm, and $a_{LS}=0.65$ fm. This resulted in spectroscopic strengths which also are too large and practically the same as with $r_0=1.20$, $a_0=0.75$, and $\lambda=20$. All calculations employed the conventional nonlocality parameters $\beta_d=0.54$ and $\beta_t=0.25$ for the scattered waves.

We note that work at medium energies does not remove the familiar ambiguities of DWBA, in particular with respect to predicting absolute cross sections. Normalization of curves to data is not unique, and the choice of the proper form-factor geometry is not always obvious, as shown above. Hence, in order to draw spectroscopic conclusions, much importance has to be placed on finding and resolving all fractions of a given configuration, including those at higher excitation.

C. Empirical unfolding of $p_{1/2}$-$p_{3/2}$ mixing

The proportions of $p_{1/2}$ and $p_{3/2}$ transfers to the 1^+ states can be extracted empirically (within a few percent error) from the measurements of their analyzing powers, because the latter show striking differences (see Figs. 11 and 12). DWBA calculations were of limited use in unfolding the mixing of different j transfers, because they did not fit the data above $\theta_{c.m.}\sim 20°$. Therefore, we decomposed $p_{1/2}$ and $p_{3/2}$ contributions by using two empirical curves, derived from pure $p_{3/2}$ and $p_{1/2}$ transfers. Figure 13 shows the analyzing powers (A_y) of

TABLE I. Levels populated in $^{15}N(d,t)^{14}N$. An asterisk denotes an undetermined value.

E_x (MeV±keV)	J^π	T	E_x (MeV±keV)	l	j	C^2S[c]	J^π, T	$(d\sigma/d\Omega)_{max}$[b] (μb/sr)
Prior work[a]						Current results		
0.000	1^+	0	0.000	1	$\{\frac{1}{2}$	1.243±0.089		5942±184
					$\frac{3}{2}$	0.100∓0.075		
2.313	0^+	1	2.312±2	1	$\frac{1}{2}$	0.472±0.009		2049±78
3.948	1^+	0	3.946±4	1	$\{\frac{1}{2}$	0.177±0.044		2921±98
					$\frac{3}{2}$	0.479∓0.039		
4.915±1	0^-	0	4.910±6	(0)	$\frac{1}{2}$	(0.008±0.001)		18.0±3.4
5.106	2^-	0	5.102±5	2		0.056±0.007		485±19
5.691	1^-	0	5.689±4	2	$\frac{3}{2}$	0.010±0.001		50.8±4.0
5.834	3^-	0	5.832±3	2	$\frac{5}{2}$	0.045±0.012		315±12
6.203	1^+	0	6.202±3	1	$\frac{3}{2}$	0.047±0.0007		201±8.7
6.446	3^+	0	6.443±6	*		<(0.002)		6.4±2.2
7.029	2^+	0	7.028±2	1	$\frac{3}{2}$	1.108±0.025		4700±116
7.967	2^-	0	7.966±4	(2)		(0.017±0.005)		12.6±1.1
8.490±1	4^-	0	8.491±4	*				40.2±4.3
9.172	2^+	1	9.173±5	1	$\frac{3}{2}$	0.423±0.008		1717±77.7
9.389±1	2^-	0	9.388±5	(2)		(0.022±0.003)		52.9±31.3
9.509±3	2^-	1	9.522±21	(2)		(0.007±0.001)		14.8±3.8
9.703±4	1^+	0	9.708±8	1	$(\frac{3}{2})$	(0.005±0.001)		7.2±3.2
10.101±15	$1^+,2^+$	0	10.108±6	1	$\frac{3}{2}$	0.061±0.003	$(2)^+$	65.5±17.4
10.432±7	2^+	1	10.440±6	1	$\frac{3}{2}$	0.388±0.013		1487±64
11.050±5	3^+		11.056±8	*		<(0.017)		30.6±2.9
11.24±15	3^-	0	11.252±9	(2)	$\frac{5}{2}$	(0.016±0.001)		20.6±13.7
11.513±1	$2^+,3^+$		11.515±10	*		<(0.006)	(3^+)	18.7±13.1
11.741±6	$1^-,2^-$		11.754±11	2	$\frac{3}{2}$	(0.014±0.001)		29.8±14.9
12.495±9			12.505±10	1	$\frac{3}{2}$	0.129±0.011	$(1^+,1)$	430±81
12.813±4	4^-		12.812±13	*				49.2±4.8
13.192±9	3^+		13.186±21	*		<(0.015)		25.4±5.7
13.74±10	1^+	1	13.732±16	1	$\frac{3}{2}$	0.452±0.011		1347±66
14.59±30			14.57±23	*				25.5±3.0
14.86±30			14.90±21	(2)	$(\frac{5}{2})$	(0.025±0.002)		38.3±9.8
15.70±50			15.63±66	(2)	$(\frac{5}{2})$	(0.037±0.003)		54.1±14.8
16.21±20			16.15±128	*				35.4±12.1
17.03±50	3^-	0+1	16.99±21	(2)	$(\frac{5}{2})$	(0.034±0.003)		63.1±6.9
17.31±30	4^+	0+1	17.28±37	*		<(0.017)		22.4±4.9
17.85±50	$4^+,3^-$	0+1	17.88±30	(2)	$(\frac{5}{2})$	(0.045±0.005)	(3^-)	57.3±17.7
18.53±80	$2^+,3^-$	0+1	18.51±30	1	$\frac{3}{2}$	0.043±0.007	$(2^+,1)$	69.5±18.7

[a]Reference 11.
[b]Maximum cross section observed, usually at 7°.
[c]Errors shown reflect statistics only.

four known $p_{3/2}$ transfers, three to 2^+ states of ^{14}N at excitation energies of 7.029, 9.172, 10.432 MeV, and one to the ground state of ^{11}C, which is a $\frac{3}{2}^-$ state.

To obtain a standard $p_{3/2}$ A_y curve we took the weighted average of these four data sets. In this simple averaging procedure we are neglecting the Q (and mass) dependence and any systematic errors for A_y. To account for this problem, we assign an added uncertainty $\Delta A_y = \pm 0.02$ for the average of the measured A_y. Figure 14 shows the deduced "standard" A_y shape for a $p_{3/2}$ transfer, with the estimated errors, which served as a templet for pure $p_{3/2}$ transfer. Similarly, for pure $p_{1/2}$ transfers, we use the $^{15}N(\vec{d},t)^{14}N$ transition to the 2.313 MeV 0^+ state and the $^{12}C(\vec{d},t)^{11}C$ transition to the 2.000 MeV $\frac{1}{2}^-$ state. The A_y for these two states are shown in Fig. 15. Figure 16 shows the "standard" curve constructed in the same way as above, which served as a templet for $p_{1/2}$ admixtures. The extraction of relative contributions of $p_{1/2}$ and $p_{3/2}$ transfers to the 1^+ states was done by performing least-squares fits of the templet curves to the data.

Our procedure neglects the cross terms which arise in the more appropriate adding of amplitudes. In order to test the validity of this approximation the mixing of $p_{1/2}$,

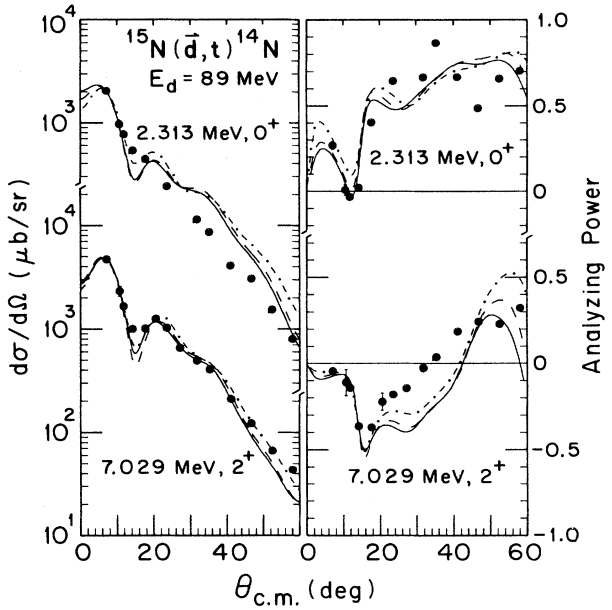

FIG. 11. Comparison of finite-range and zero-range DWBA calculations for $p_{1/2}$ and $p_{3/2}$ neutron pickup. The dot-dashed curves represent zero-range DWBA calculations. The dashed curves represent finite-range DWBA calculations with only an S state (d,t) form factor. The solid curves represent our most complete calculations and represent finite-range DWBA calculations with S and D components of the form factors.

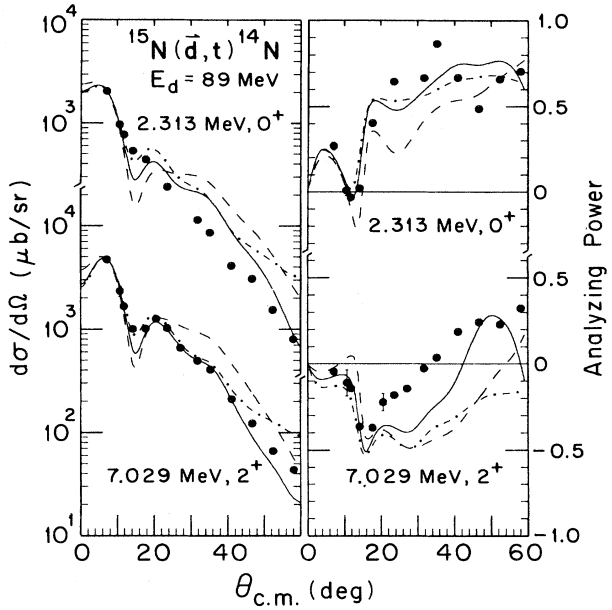

FIG. 12. Comparison of finite-range DWBA calculations using various OM parameters for tritons. The dashed curve, the dot-dashed curve and the solid curve represent the calculations with the shallow potential (S), the extrapolated Becchetti-Greenlees potential (BG) and the deep potential (D) of Table II, respectively.

$p_{3/2}$ DWBA amplitudes was compared with the mixing of DWBA analyzing powers intensities. For $^{15}N(\vec{d},t)$ at 89 MeV the results were nearly identical.

We note that a similar unfolding of j contributions was possible in the $^{15}N(\vec{^3He},\alpha)^{14}N$ experiment at 33 MeV. Although absolute spectroscopic factors are generally harder to deduce for $(\vec{^3He},\alpha)$ transfers, the $p_{1/2}$-$p_{3/2}$ mixing ratios obtained in Ref. 8 are almost identical to those of this study (see Table III).

V. DISCUSSION

A. Assignments for individual levels

Cross sections for the 0^+, 1^+, and 2^+ levels shown in Figs. 3–5 clearly exhibit the characteristics of $l=1$ transitions. The structure of the angular distributions suggests a j effect difference between the 2.313 MeV 0^+ state ($p_{1/2}$ pickup) and any 2^+ states ($p_{3/2}$ pickup), even for $\sigma(\theta)$. The empirical $p_{1/2}$ pickup data show a steeper slope (although the DWBA calculations differ very little). On the other hand, the shapes of all cross sections for 2^+ states with a characteristic secondary peak at $\theta_{c.m.} \sim 20.6°$ look very similar to each other. Among the 1^+ states (which can be excited by both $p_{1/2}$ and $p_{3/2}$ pickup) the g.s. distribution is steep, similar to that of the 2.313 MeV 0^+ state, indicating that $p_{1/2}$ pickup is dominant for this state, whereas all other distributions are similar to that of the $p_{3/2}$ pickup distribution, including the characteristic peak at $\theta_{c.m.} \sim 20.6°$.

It is evident from Fig. 12 that shapes of the analyzing powers for the $p_{1/2}$ (e.g., 2.313 MeV, 0^+ state) and $p_{3/2}$

TABLE II. Optical-model potential parameters used in DWBA calculations.

Set		V	r_0	a_0	W_S	W_D	r_I	a_I	V_{LS}	r_{LS}	a_{LS}	r_c	Ref.
1	d	68.126	1.17	0.858	7.805	6.682	1.325	0.663	4.779	1.07	0.66	1.3	13
2		76.95	1.15	0.79		9.62	1.33	0.685				1.3	18
3		61.5	1.25	0.667		10.57	1.096	0.84				1.3	19
4		78.9	1.05	0.78		8.14	1.32	0.86				1.3	23
5	$t(D)$	205.0	1.08	0.72		14.9	1.35	0.67	11.34	0.73	0.67	1.3	15
6	(S)	99.2	1.24	0.77	1.24	15.8	1.40	0.71	6.6	0.91	0.49	1.3	15
7	(BG)	150.0	1.20	0.72	17.0		1.40	0.84	5.0	1.20	0.72	1.3	16

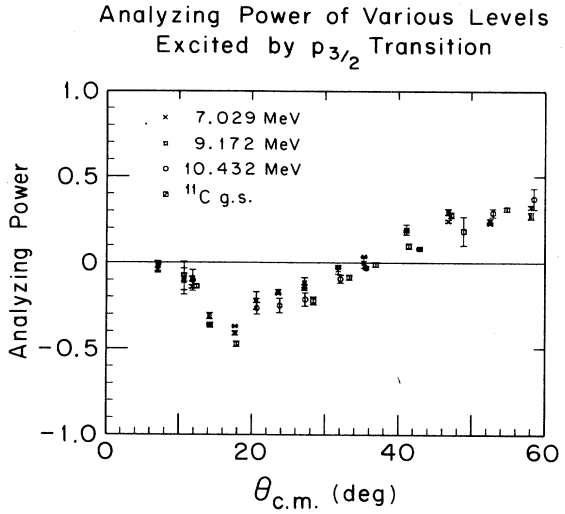

FIG. 13. Comparison of $p_{3/2}$ analyzing powers for the strong transitions to the 2^+ levels of ^{14}N at 7.029, 9.172, and 10.432 MeV, and the ^{11}C g.s. ($\frac{3}{2}^-$). (Selection rules require pure $p_{3/2}$ transfer to 2^+ states in one-step pickup reactions.)

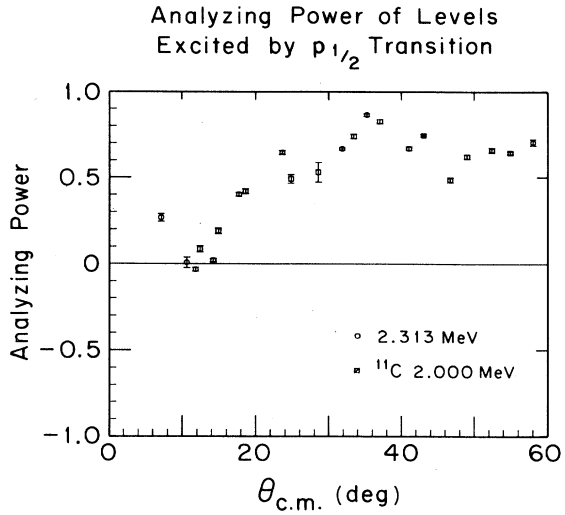

FIG. 15. Analyzing powers for transitions to the $J^\pi=0^+$ ^{14}N level at 2.313 MeV and the $J^\pi=\frac{1}{2}^-$ ^{11}C level at 2.000 MeV. (These levels must be excited by pure $p_{1/2}$ pickup in one-step transfer.)

pickup (e.g., 7.029 MeV, 2^+ state) differ even more strikingly. For a $p_{1/2}$ pickup A_y is positive (except near $\theta_{c.m.} \approx 12°$) in the entire observed range of 7°–58°. On the other hand, for a $p_{3/2}$ pickup A_y is negative for all small angles up to about 34°, when it becomes positive and remains positive, but small, up to the maximum angle of measurement. The zero crossing point shifts towards larger angles for larger excitation energy, as can be seen from the A_y distributions corresponding to the 7.029, 9.172, and 10.432 MeV 2^+ states. This feature is qualitatively (but not accurately) reproduced by DWBA calculations.

The A_y for the g.s. (1^+) resembles that of the 2.313 (0^+) state, confirming the predominance of $p_{1/2}$ pickup. The A_y distribution for the 3.948 MeV 1^+ state shows a strong mixing of $p_{1/2}$ and $p_{3/2}$ pickups (Fig. 17), whereas the other 1^+ A_y distributions show primarily $p_{3/2}$ pickup.

If the j templets discussed above are used, the best A_y fit to the ground-state transition requires an (8.4±6.3)% $p_{3/2}$ admixture. The 3.948 MeV state shows a strong $p_{1/2}$ admixture of (24.3±6.0)%. The 1^+ states at 6.203

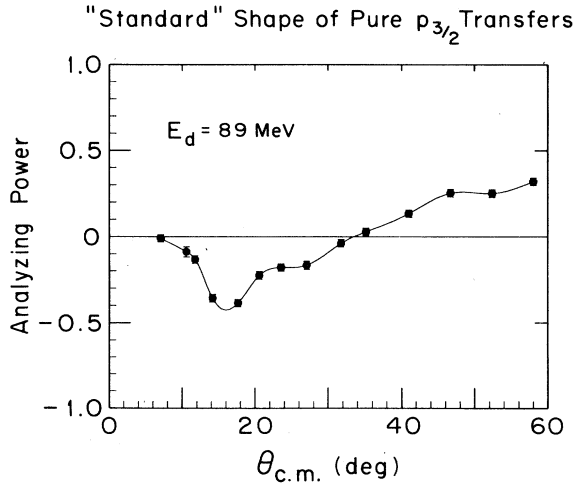

FIG. 14. Deduced "standard" shape for the analyzing powers for pure $p_{3/2}$ pickups, obtained by averaging the points of Fig. 13. The solid curve represents a cubic spline fit to the point averages, which was used for the unfolding of $p_{1/2}$-$p_{3/2}$ mixing.

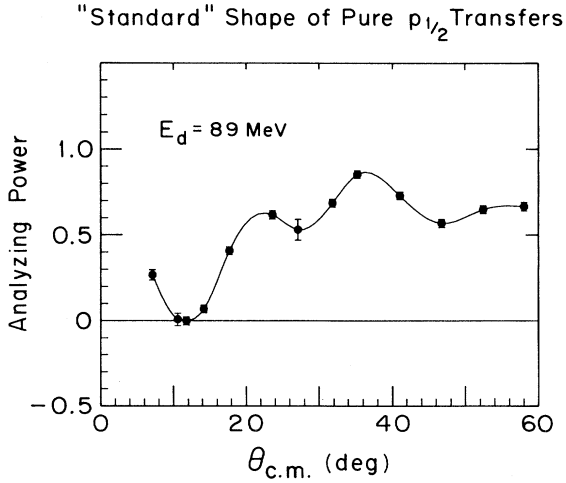

FIG. 16. "Standard" shape for the analyzing powers for pure $p_{1/2}$ pickup, obtained by averaging the points of Fig. 15 (see Sec. IV). The solid curve represents a cubic spline fit to the points.

TABLE III. Comparison of the Cohen-Kurath calculations with experiments.

Cohen-Kurath calculation					Present work				Ref. 8
$E_{calc.}$	J^π, T	nlj	CFP[a]	% mixing	E_x	J^π, T	nlj	% mixing	% mixing
0.000	1^+0	$1p_{3/2}$	0.0542	2.2	0.000	1^+0	$1p_{3/2}$	8.4±6.3	~10
		$1p_{1/2}$	−0.3601	97.8			$1p_{1/2}$	91.6∓6.3	~90
2.690	0^+1	$1p_{1/2}$	0.3376		2.313	0^+1	$1p_{1/2}$		
3.616	1^+0	$1p_{3/2}$	0.2434	93.5	3.948	1^+0	$1p_{3/2}$	75.7±6.0	70
		$1p_{1/2}$	0.0642	6.5			$1p_{1/2}$	24.3∓6.0	30
					6.203	1^+0	$1p_{3/2}$	100.0	
							$1p_{1/2}$	0.0	
6.991	2^+0	$1p_{3/2}$	−0.3371		7.029	2^+0	$1p_{3/2}$		
					10.101	2^+0	$1p_{3/2}$		
9.524	2^+1	$1p_{3/2}$	−0.5704		9.172	2^+1	$1p_{3/2}$		
					10.432	2^+1	$1p_{3/2}$		
11.783	1^+1	$1p_{3/2}$	−0.4523	100.0	12.495	$(1^+)(1)$	$1p_{3/2}$	94.8±9.6	dominant
		$1p_{1/2}$	0.000	0.0			$1p_{1/2}$	5.2∓9.6	
					13.74	1^+1	$1p_{3/2}$	100.0	100.0
							$1p_{1/2}$	0.0	0.0
15.238	1^+0	$1p_{3/2}$	−0.0776	70.25					
		$1p_{1/2}$	−0.0505	29.75					
16.323	0^+1	$1p_{1/2}$	0.1497						
17.879	2^+1	$1p_{3/2}$	−0.1246		18.53	2^+1	$1p_{3/2}$		

[a]Coefficient of fractional parentage.

and at 13.74 MeV are consistent with 100% $p_{3/2}$ pickup within uncertainties of 7–8%. Figure 17 shows the analyzing powers and fits obtained by mixing the standard $p_{1/2}$ and $p_{3/2}$ curves in the optimal ratio for the ground state and the 3.948 MeV state.

In the literature[11] we find the 10.101 MeV level assigned as $J^\pi=1^+$ or 2^+ with $T=0$. In the present experiment we deduce from the analysis of analyzing powers, that it is excited by a pure $p_{3/2}$ transition within a 9% uncertainty. It seems that the $1p_{3/2}$ ($J^\pi=2^+$, $T=0$) strength predicted by Cohen and Kurath for a level at 6.991 MeV is shared by the 10.101 and 7.029 MeV levels. This is supported by the sum of the spectroscopic strengths (1.16±0.03) for these two levels as compared to the predicted spectroscopic strength of 1.25 for a 6.991 MeV level. Hence we suggest $J^\pi=2^+$ for the 10.101 MeV level. The $J^\pi=2^+$, $T=1$ state predicted for 9.524 MeV also appears to be split between two $J^\pi=2^+$, $T=1$ levels observed at 9.172 and 10.432 MeV. This conclusion was also reached from different nuclear reactions.[7,30] Our ratio of the spectroscopic strengths for the 9.172 and 10.432 MeV states is 1.09±0.04, and agrees, within errors, with Snelgrove and Kashy's ratio of 1.25±0.2.

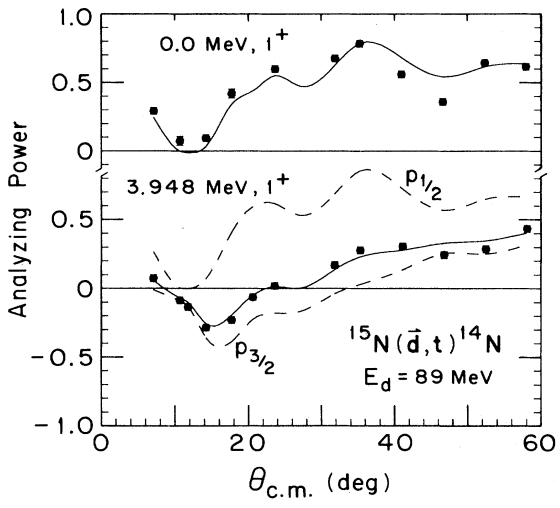

FIG. 17. Analyzing powers for transitions leading to the 1^+ ground and 3.948 MeV states of ^{14}N. The solid curves represent mixtures of the standard A_y curves (dashed curves) that yield the best fit to the data. The A_y for the g.s. is very close to that of standard $p_{1/2}$ pickup of Fig. 16, indicating that this level is excited predominantly by $p_{1/2}$ pickup. (See Sec. V for details.)

The 12.495 MeV state had no previous J^π or T assignment. From Fig. 4 it is clear that the angular distribution of σ is that of a $l=1$ transition. The angular distribution of the A_y again corresponds to dominant $p_{3/2}$ pickup. The A_y decomposition method suggests a (5.2±9.6)% $p_{1/2}$ admixture. Because of the strong $p_{3/2}$ component, this state must be either a 1^+ or 2^+ state. Cohen and Kurath predicted a $J^\pi=1^+$, $T=1$ level at 11.783 MeV. Some of this strength appears at 13.74 MeV. The present work suggests that the predicted strength for the 11.783 MeV level is split between the 12.495 and 13.74 MeV levels. The sum of the measured spectroscopic strengths for these two levels is 0.58±0.02, as compared to the predicted strength of 0.75. The 10.44 MeV level of ^{14}C in the $^{15}N(\vec{d},{}^3He)^{14}C$ work by Kaschl *et al.*[31] corresponds to the 12.495 MeV level of ^{14}N and thus supports our $T=1$ preference for this state. This preference is further supported by the absence of this peak in a $^{16}O(d,\alpha)^{14}N$ spectrum taken during this experiment. We tentatively assign $J^\pi=1^+$, $T=1$ for the 12.495 MeV level via a 100% $p_{3/2}$ transition. The $^{16}O(d,\alpha)^{14}N$ work by Holbrow *et al.*[32]

together with the work by Kaschl *et al.* supports the $T=0$ values taken from the literature.

In addition to the stronger and well-known neutron pickup transitions we saw a number of weak transitions that may not be one-step transfers. In the tables, their l transfers and spectroscopic factors are listed in parentheses; and the corresponding DWBA calculations are shown as dotted lines in Figs. 8–10, since it is uncertain to which degree higher-order processes contribute. The excitation of negative-parity levels with $J^\pi \leq 3^-$ levels suggests some $s_{1/2}$, $d_{3/2}$, and $d_{5/2}$ admixtures in the ground state of ^{15}N. In the present study we identify nine such states (Figs. 7 and 8). They are all weak and only a few will be discussed. The angular distributions of σ for the 2^- level at 5.106 MeV and the 3^- level at 5.834 MeV agree with the DWBA prediction for $l=2$ transfer (Fig. 7). As before, calculated shapes of the analyzing powers do not agree with the data past $\theta_{\text{c.m.}} \sim 20°$, but do not contradict the conclusion that these two levels are excited by $1d_{5/2}$ pickup. The shape of the cross section for the 5.691 MeV, 1^- state is close to the DWBA prediction for $1d_{3/2}$ pickup with a positive and unique A_y. We tentatively assign $d_{3/2}$ transfer for this state.

The 0^- level at 4.915 MeV can only be excited by $2s_{1/2}$ neutron pickup in a one-step direct reaction picture, but the shape of the angular distribution is poorly reproduced by the $l=0$ DWBA calculation. The 11.513 MeV state previously assigned $J^\pi=2^+$ or 3^+ shows a cross section similar to the other three 3^+ states in Fig. 9 and is inconsistent with $l=1$ or 3 pickups. The A_y of the 11.513 MeV state agrees with that of the 13.192 MeV level within experimental error.

We took spectra up to an excitation energy of 24 MeV in search of any additional high-lying p or s,d strength. Six weak ^{14}N levels, above 13.74 MeV, have been identified by comparing their excitation energies and characteristic widths with those from the nuclear data tables.[11] For the levels at 14.90 and 16.15 MeV, the characteristic widths disagree with those of known states. The level seen at 18.51 MeV (Fig. 5) deserves additional comment. In the nuclear data tables two levels are listed at 18.53 MeV; one with $J^\pi=2^+$ and a width of 410±80 keV, and the other with $J^\pi=3^-$ and a width of 310±60 keV. We find that the level at 18.51 MeV agrees with $l=1$ and has a width of 450 keV, suggesting that we excited the 2^+ state. The angular distributions of $\sigma(\theta)$ and A_y (Fig. 5) are indicative of a $p_{3/2}$ transfer. This assignment is further supported by the prediction of a weak $J^\pi=2^+$, $T=1$ level at 17.879 MeV by Cohen and Kurath. We assume $T=1$ for this state in accordance with the above prediction.

None of the seven angular distributions for cross sections and A_y for the weak states shown in Fig. 6 suggests $l=1$ transfer. Instead, the analyzing powers for the levels at 14.59 and 14.86 MeV agree rather well with those for the 12.813 MeV $J^\pi=4^-$ level and 16.99 MeV $J^\pi=3^-$ level, respectively. These weak levels are probably excited by multistep processes. The statistics are too poor for any further conclusion.

Above the 18.51 MeV peak we see a nearly flat continuum [Fig. 2(b)], with indication of four bumps of widths of about 0.75, 0.5, 1.0, and 0.5 MeV, respectively, between 19.0 and 22.0 MeV. The shapes of σ and A_y of these four regions look very much alike (Fig. 18) and are inconsistent with $l=1$ transitions. Hence, if there is $l=1$ strength in this continuum it must be weak. Similarly, the angular distribution differ from $l=2$ predictions. These broad bumps might come from $1s_{1/2}$ pickup which could lead to very broad peaks. The DWBA calculations for $1s_{1/2}$ pickup are shown in Fig. 18 and represent the cross sections fairly well. The total implied $1s_{1/2}$ spectroscopic strength for this continuum is 2.22±0.06, which is only 10% higher than the shell-model limit of 2.0.

B. Spectroscopic sums

It is to be noted that our total $l=1$ g.s. strength of 1.34±0.12 is comparable with the predicted (total of $p_{3/2}$ and $p_{1/2}$) value of 1.46 and the Snelgrove-Kashy value of 1.27±0.09. Also, the total extracted strength for the 3.948 MeV state (0.66±0.06) agrees with the Cohen-

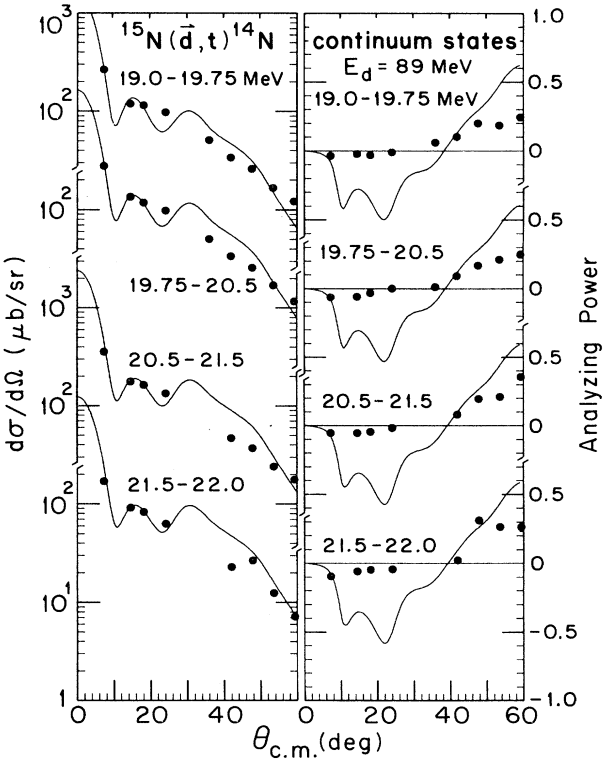

FIG. 18. Angular distributions of cross sections and analyzing powers of sections of the continuum excited in this reaction above the broad 18.51 MeV peak. The 19.0–22.0 MeV excitation region was divided into four subregions as shown. Solid curves represent DWBA calculations for pickup of the deeply bound $1s_{1/2}$ neutrons. While the A_y are not well predicted, the cross section are in better agreement with the data than calculations for any other l.

Kurath prediction and Snelgrove-Kashy value, which are 0.70 and 0.60±0.07, respectively. For $p_{1/2}$ transitions, we find $\sum C^2S(p_{1/2};J^\pi=0^+)=0.472\pm0.009$ and $\sum C^2S(p_{1/2};J^\pi=1^+)=1.420\pm0.099$; both of these values are about 5% below the sum rule, which are 0.5 and 1.5, respectively, for these orbitals.

For $p_{3/2}$ transitions, the strength seen is about 19% below the sum rule for both $J^\pi=1^+$ and 2^+ final states, the sum being $\sum C^2S(p_{3/2};J^\pi=1^+)=1.212\pm0.086$ and $\sum C^2S(p_{3/2};J^\pi=2^+)=2.023\pm0.030$, compared to the shell-model limits of 1.5 and 2.5, respectively. The total $l=1$ strength is $\sum C^2S(l=1)=5.127\pm0.135$. A small part of the missing strength is found in three $l=2$ transitions, one $d_{3/2}$ transition leading to a final state with $J^\pi=1^-$, and two $d_{5/2}$ transitions leading to final states with $J^\pi=2^-$ and 3^-. The sum of $l=2$ strengths is $\sum C^2S(l=2)=0.111\pm0.014$. This shows that the total observed $l=2$ strength is only 2.2% of the total observed $l=1$ strength. This observation disagrees with the predictions of Glaudemans *et al.*[4] who calculated *s-d* admixtures of about 40%. Assuming that the DWBA normalization is reliable, the missing strength (0.76) must lie at excitation energies at or above 19.0 MeV.

We have taken pains to compute realistic form factors and extract the best spectroscopic factors; however, the DWBA approach at medium energies is a rough approximation and cannot always be trusted to give reliable *absolute* spectroscopic factors. Hence, it is instructive to look at the distribution of the spectroscopic strength for various orbits as a function of excitation energy in order to check for any signs for its spreading to high excitations. Figure 19 shows no evidence of unusual splitting or spreading and supports the assumption that the absolute $p_{1/2}$ and $p_{3/2}$ strengths have been mapped to good accuracy. It also illustrates graphically the very small *s-d* admixtures seen.

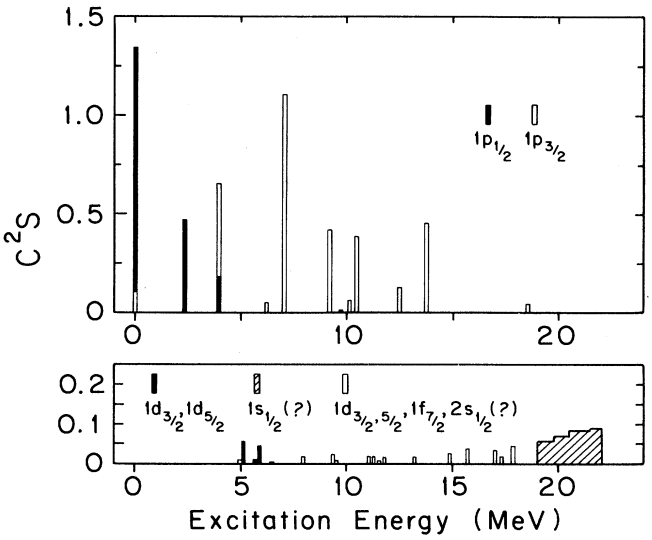

FIG. 19. Distribution of spectroscopic strengths with excitation energy. The data do not suggest any substantial *s,d* strength below 20 MeV, nor much spreading and mixing of $p_{1/2}$ and $p_{3/2}$ strengths. Note the expanded scale for the lower graph and that the 1*s* continuum C^2S values for regions of arbitrary widths in excitation energy, are maximum values and are likely to include significant background contributions.

VI. EMPIRICAL EFFECTIVE INTERACTIONS

Extraction of empirical $l=1$ matrix elements from transfer data requires that essentially all $l=1$ strength has been found. Cohen and Kurath (CK) predicted six strong *p*-shell levels below 14 MeV. We observed ten strong levels with characteristic $l=1$ transitions below 14 MeV. Table III compares the predictions of CK and the present experimental observations of correlated quantities. We note that, of the 1^+ states, the 3.948 MeV state shows significantly stronger $p_{1/2}$-$p_{3/2}$ mixing than predicted. This means other differences from CK should be expected. Spectroscopic $l=1$ strengths extracted by matching the experimental and calculated cross sections are compared in Table IV with the experimental values of Snelgrove and Kashy, the Birmingham work and the CK predictions.

Given the spin assignments and spectroscopic strengths for states containing the configurations $(p_{1/2}p_{1/2})$ or $(p_{3/2}p_{1/2})$, we can calculate the residual interaction matrix elements for both of these configurations.[5] We determine the energy centroid $\mathcal{E}_{\text{cent}}$ of each J and T by weighting each level energy with its spectroscopic strength. Then according to Eq. (1) we subtract the unperturbed multiplet energy from the centroid energies. The unperturbed multiplet energy for the $(p_{1/2},p_{1/2},p_{1/2}p_{1/2})$ configuration is given by

$$E_0(p_{1/2})=B(^{15}\text{N})+B(^{15}\text{O})-B(^{14}\text{N})-B(^{16}\text{O}) ,$$

where B stands for binding energy (mass excess). For the $P_{3/2}p_{1/2}$, $p_{3/2}p_{1/2}$, configuration $E_0(p_{3/2})$ is given by

$$E_0(p_{3/2})=B(^{15}\text{N}^*)+B(^{15}\text{O})-B(^{14}\text{N})-B(^{16}\text{O}) .$$

The asterisk denotes that the nucleus listed is excited to its single-particle (j) level. We obtain $E_0(p_{1/2})=4.834$ MeV and $E_0(p_{3/2})=11.158$ MeV . Deduced centroid energies and residual interaction matrix elements are listed in Table V where the column $E(J)_{\text{min}}$ shows firm lower limits for the six diagonal matrix elements for $(p_{1/2}p_{1/2})$ and $(p_{3/2}p_{1/2})$ configurations. We call the deduced value $E(J)_{\text{min}}$ because any missing strength has to be at higher excitation; hence, the value given represents the lower limit of the true value. We find that these values are close to the CK results except for two matrix elements: the $(p_{1/2}p_{1/2})$ configuration with $J^\pi=0^+$ and $T=1$ and the $(p_{3/2}p_{1/2})$ configuration with $J^\pi=1^+$, $T=1$.

TABLE IV. $^{15}N(d,t)^{14}N$ spectroscopic factors compared with other work.

lj	J^π	T	E_x (MeV)	C^2S (present) $(d,t)\pm$error	C^2S (Ref. 7) $(p,d)\pm$error	C^2S (Ref. 8) (^{3}He,α)	C^2S (Ref. 1) *CK*, theory
	0^+	1	2.313	0.472±0.009	0.50±0.03	0.61	0.418
	0^+	1	(16.323)				0.082
$p_{1/2}$	1^+	0	0.000	1.243±0.089	1.27±0.09	0.864	1.427
	1^+	0	3.948	0.177±0.044		0.192	0.045
	1^+	0	(15.238)				0.028
	1^+	0	0.000	0.100±0.075		0.096	0.032
	1^+	0	3.948	0.479±0.039	0.60±0.07	0.45	0.652
	1^+	0	6.203	0.047±0.001	0.03±0.01		
	1^+	0	9.703	(0.005±0.001)			
	1^+	0	(15.238)				0.066
	1^+	(1)	12.495	0.129±0.011		0.23	0.750
	1^+	1	13.74	0.452±0.011	0.81±0.06	0.97	
$p_{3/2}$	2^+	0	7.029	1.108±0.025	1.02±0.07	0.97	1.250
	2^+	0	10.101	0.061±0.003	0.03±0.01		
	2^+	1	9.172	0.423±0.008	0.49±0.06	0.59	1.193
	2^+	1	10.432	0.388±0.013	0.39±0.05	0.50	
	2^+	1	18.53	0.043±0.007			0.057
$\sum_{l=1} C^2S$:				5.127	5.14	5.472	6.0

As pointed out in detail in Ref. 5, two-nucleon matrix elements derived from a single (transfer) reaction tend to suffer from systematic errors unless *all* fractions of a multiplet have been identified. For particle-particle or hole-hole states (as in the present case) configuration mixing moves some strength to high excitations where it is hard or impossible to separate from more dominant transitions. On the other hand, low-lying strength is hard to miss; hence, the empirical matrix elements derived in such cases are generally too attractive. In Table V we account for this effect by calling the uncorrected effective interaction matrix elements $E(J)_{\min}$.

Systematic errors in transitions to particle-hole states have the opposite sign; hence, it has been possible to find good upper and lower limits for effective interactions if both types of transitions have been studied.[5] In the $^{15}N(\vec{d},t)^{14}N$ case only the lower limits for $E(J)$ can be given with confidence. In column 8 of Table V the upper

TABLE V. Matrix elements of p-shell residual interactions.

Configuration	J^π	T	E_x (MeV)	C^2S	$\mathcal{E}_{\text{cent}}$[a]	$E(J)_{\min}$[b]	$E(J)_{\max}$[c]	$E(J)_{\text{av}}$[d]	CK value
	0^+	1	2.313	0.472	2.313	−2.521	−1.587	−2.054	−0.26
$p_{1/2}p_{1/2}$	1^+	0	0.000	1.243	0.492	−4.342	−3.355	−3.848	−4.15
			3.948	0.177					
			0.000	0.100					
	1^+	0	3.948	0.479	3.487	−7.671	−5.106	−6.388	−6.22
			6.203	0.047					
	1^+	1	12.495	0.129	13.463	2.305	3.553	2.929	0.92
			13.740	0.452					
$p_{3/2}p_{1/2}$	2^+	0	7.029	1.108	7.189	−3.969	−3.203	−3.586	−4.00
			10.101	0.061					
			9.172	0.423					
	2^+	1	10.432	0.388	10.216	−0.942	1.840	0.449	−0.96
			18.530	0.043					

[a]Energy centroids of levels for a given configuration $|j_1 j_2\rangle J^\pi, T$.
[b]Lower limits of the matrix elements for various configurations as described in Sec. VI. Unperturbed multiplet energies used are $E_0(p_{1/2})=4.834$ MeV, $E_0(p_{3/2})=11.158$ MeV.
[c]*Tentative* upper limts of the matrix elements, as described in Sec. VI.
[d]Our best estimates (see Sec. VI).

limits $E(J)_{max}$ are estimated on the basis of missing spectroscopic strength. Here we assigned the missing strength in each category to 19.0 MeV in order to estimate the systematic effect of possible high-lying components. The somewhat arbitrary value of 19.0 MeV was chosen because we could not identify any $l=1$ transition above the 18.53 MeV peak. These values thus represent tentative upper limits of the matrix elements, with the true value for $E(J)$ somewhere between $E(J)_{min}$ and $E(J)_{max}$.

Upper limits for $E(J)$ estimated on the basis of missing spectroscopic strength are strongly model dependent and are suggestive rather than conclusive. As shown in Table V, $[E(J)_{max}-E(J)_{min}]$ tends to be of order 1 MeV. In order to facilitate comparison with other work we list the average of the two extremes, $E(J)_{av}$, as our "best estimate" and assign an uncertainty of about 0.8 MeV. This estimated error generally brackets the reliable lower limits for $E(J)$, but does not have the character of a maximum error or a standard deviation.

In spite of the large uncertainties given and the weak upper limits, the "best values" for the $\langle p_{1/2}p_{1/2};01|p_{1/2}p_{1/2}\rangle$ and $\langle p_{3/2}p_{1/2};11|p_{3/2}p_{1/2}\rangle$ matrix elements differ substantially (by about 2 MeV) from previously calculated ones (see Table V), whereas the four other diagonal matrix elements are in good agreement with the Cohen-Kurath values. The disagreement is particularly significant for the latter matrix element since the new value is about 2 MeV less attractive, and it is difficult to fault the empirical value for a systematic error in this direction. Hence, the $^{15}N(\vec{d},t)$ analysis suggests that the CK $T=1$ matrix elements for $(p_{1/2})^2_{0^+}$ and $(p_{1/2}p_{3/2})_{1^+}$ must be modified significantly.

VII. SUMMARY AND CONCLUSIONS

$^{15}N(\vec{d},t)^{14}N$ spectra were investigated up to an excitation energy of 24.0 MeV in ^{14}N in search of high-lying p or s,d strength. Overlapping data from the QDDM and the K600 spectrographs were consistent, after careful normalization. Above the known broad 13.74 MeV peak, we identified one more peak, at 18.51 MeV, which is excited by $l=1$ transition. Above this peak, we see only a continuum which is not measurably affected by $l=1$ strength. Also, we have not found any $l=2$ strength in the continuum. The $1d$ and $2s$ spectroscopic sums for discrete states total only 0.12. If all weak (but doubtful) transfers are added which might possibly be explained by $l=2$, the sum increases to 0.34. No significant $l=3$ strength was seen anywhere. If the continuum is to be explained by direct neutron pickup to unbound states, the best assumption appears to be that in the region of observation it is dominated by excitation of the $1s_{1/2}$ shell. Hence, our data offer no support for the calculations of Ref. 4.

The discrimination between pure $p_{1/2}$ and pure $p_{3/2}$ transition analyzing powers at 89 MeV was found to be excellent. Hence, an empirical unfolding of contributions of different j transfers for the 1^+ states became possible, although DWBA calculations were not used because they failed to reproduce the analyzing powers above $\theta_{c.m.}\sim 20°$. Agreement of DWBA calculations with observed differential cross-sections was fairly good. The total spectroscopic strength deduced was 88% of the shell-model sum rule.

The CK predictions[1] agree fairly well with many of the present experimental observations. However, several levels predicted by CK are found to be split. The predicted weak mixing of $p_{1/2}$-$p_{3/2}$ components for the 1^+ states is consistent with observation, except for the state at 3.948 MeV, where much more mixing is found than predicted. Four of the extracted experimental values of the p^2 residual interaction matrix elements are consistent with CK results, but the $T=1$ matrix elements for the $(p_{1/2}p_{1/2})_{0^+}$ and $(p_{3/2}p_{1/2})_{1^+}$ differ by over 1 MeV. These large differences suggest great caution in the future use of the CK values.

ACKNOWLEDGMENTS

We wish to thank Dr. K. F. von Reden, Dr. R. D. Rosa, and William Temple for helping during different phases of data taking. The authors are indebted to the cyclotron crew members of IUCF for their cooperation, and to W. R. Lozowski for preparing the targets. We also acknowledge helpful discussions with Dr. C. M. Vincent. This work was supported in part by the National Science Foundation.

[1] S. Cohen and D. Kurath, Nucl. Phys. **A73**, 1 (1965); **A101**, 1 (1967).

[2] P. S. Hauge and S. Maripuu, Phys. Rev. C **8**, 1609 (1973).

[3] A. G. M. van Hees and P. W. M. Glaudemans, Z. Phys. A **314**, 323 (1983); **315**, 223 (1984).

[4] P. W. M. Glaudemans, in *Proceedings of the International Symposium on Nuclear Shell Models, Drexel University, 1984* (World-Scientific, Singapore, 1984), pp. 2–19; N. A. F. M. Poppelier, L. D. Wood, and P. W. M. Glaudemans, Phys. Lett. **157B**, 120 (1985).

[5] W. W. Daehnick, Phys. Rep. **96**, 317 (1983); also see J. P. Schiffer and W. W. True, Rev. Mod. Phys. **48**, 191 (1976).

[6] N. Austern, Nucl. Phys. **A292**, 190 (1977).

[7] J. L. Snelgrove and E. Kashy, Phys. Rev. **187**, 1259 (1969).

[8] P. V. Drumm, O. Karban, A. K. Basak, P. M. Lewis, S. Roman, and G. C. Morrison, Nucl. Phys. **A448**, 93 (1986).

[9] D. A. Low, V. R. Cupps, A. K. Opper, and E. J. Stephenson, IUCF Internal Report No. 87-2, 1987. For a detailed discussion of polarization measurements see E. J. Stephenson, J. C. Collins, C. C. Foster, D. L. Friesel, W. W. Jacobs, W. P. Jones, M. D. Kaitchuck, P. Schwandt, and W. W. Daehnick, Phys. Rev. C **28**, 134 (1983).

[10] G. P. A. Berg, L. C. Bland, B. M. Cox, D. DuPlantis, D. W. Miller, K. Murphy, P. Schwandt, K. A. Solberg, E. J.

Stephenson, B. Flanders, and H. Seifert, IUCF Scientific and Technical report, 1986.
[11]F. Ajzenberg-Selove, Nucl. Phys. **A449**, 1 (1986).
[12]J. R. Comfort, fitting code AUTOFT, University of Pittsburgh (unpublished).
[13]W. W. Daehnick, J. D. Childs, and Z. Vrcelj, Phys. Rev. C **21**, 2253 (1980).
[14]P. D. Kunz and J. R. Comfort, DWUCK4 and FRUCK2: DWBA codes and instructions, University of Colorado (unpublished).
[15]K. F. von Reden, W. W. Daehnick, S. A. Dytman, R. D. Rosa, J. D. Brown, C. C. Foster, W. W. Jacobs, and J. R. Comfort, Phys. Rev. C **32**, 1465 (1985).
[16]F. D. Becchetti, Jr. and G. W. Greenlees, in *Proceedings of the Third International Symposium on Polarization Phenomena in Nuclear Reactions,* edited by H. H. Barschall and W. Haeberli (University of Wisconsin Press, Madison, Wisconsin, 1971), p. 682.
[17]H. H. Chang *et al.* Nucl. Phys. **A174**, 485 (1971).
[18]D. W. Devins *et al.*, Phys. Rev. C **24**, 59 (1981).
[19]J. P. Didelez *et al.*, Phys. Rev. C **13**, 1388 (1976).
[20]W. A. Sterrenburg *et al.*, Nucl. Phys. **A420**, 257 (1984); T. Tanabe *et al.*, J. Phys. Soc. Jpn. **41**, 361 (1976).
[21]H. H. Chang *et al.*, Nucl. Phys. **A297**, 105 (1978).
[22]M. Hyakutake *et al.*, Nucl. Phys. **A311**, 161 (1978).
[23]H. Doubre *et al.*, Phys. Lett. **29B**, 355 (1969).
[24]I. S. Towner, *A Shell Model Description of Light Nuclei* (Clarendon, Oxford, 1977), p. 293.
[25]W. W. Daehnick, M. J. Spisak, and J. R. Comfort, Phys. Rev. C **23**, 1906 (1981).
[26]W. D. M. Rae, Ph.D. thesis, Oxford University, 1976 (unpublished).
[27]W. Schütz, Z. Phys. A **237**, 69 (1975).
[28]G. R. Satchler, *Direct Nuclear Reactions* (Clarendon, Oxford, 1983), pp. 712–714.
[29]J. Streets, B. A. Brown, and P. E. Hodgson, J. Phys. G **8**, 839 (1982).
[30]G. C. Ball and J. Cerny, Phys. Lett. **21**, 551 (1966).
[31]G. Kaschl, G. Mairle, H. Mackh, D. Hartwig, and U. Schwinn, Nucl. Phys. **A178**, 275 (1971).
[32]C. H. Holbrow, R. Middleton, and W. Focht, Phys. Rev. **183**, 880 (1969).